Load resistance and failure modes of hollow-core slabs with openings: A finite element analysis

Sameer K. S. Pachalla and S. Suriya Prakash

- Design engineers typically confirm the safety of prestressed hollow-core slabs with openings based on experience or by simple stress calculations because no design guidelines exist at present for their design.
- This paper evaluates the effects of openings on the behavior of hollow-core slabs through experimental and finite element method studies by varying the number of additional strands in adjacent webs, the shear span–to–depth ratio, and opening size.
- Additional strands in webs adjacent to an opening could not completely restore the lost capacity of hollow-core slabs because the location and size of the openings plays an important role in the capacity and failure mode of the hollow-core slabs.

Hollow-core slabs are precast, prestressed concrete elements used as slab components in buildings. It is common to have openings in the slabs for various structural reasons, such as provision of columns or for facilitating the installation of mechanical, electrical, and plumbing services. Due to the limitations of their manufacturing process, prestressing strands are the only reinforcement in hollow-core slabs. Openings that require removal of small areas of concrete without cutting the prestressing strands can be termed as nonstructural openings because these openings cause no adverse effects on the strength and behavior of the slabs. Such openings are provided for small pipes and other electrical or mechanical purposes. Large openings, which require the cutting of strands, can be called structural openings. These openings reduce the capacity of hollow-core slabs significantly and alter the load-distribution paths, making these slabs a weak link in the whole assembly. Therefore, they require special attention in both analysis and design. In most cases, openings are preplanned during the design phase. In the industry, the common method of designing hollow-core slabs with openings is to provide additional strands equal to the number of strands cut for the opening. These strands are either provided in the adjacent webs or distributed uniformly in the remaining cross section. However, during construction it is not unusual to provide openings in locations where the necessary design precautions were not taken. Design engineers evaluate the effects of openings based on simple calculations using linear analysis or based on experience.

Previous researchers[1–5] have evaluated the flexural and shear behavior of hollow-core slabs under the effects of various parameters, such as the shear span–to–depth ratio *a/d* (where *a* is the shear span and *d* is the depth of the section), prestressing force, depth of slab, and shape of voids. Previous work by the authors[6–8] highlighted the effects of flexural and shear openings in reducing the ultimate strength of hollow-core slabs using full-scale experimental studies. The main parameters were the location of the opening and the *a/d* value. It was observed that a flexural opening in the slab reduced the capacity by 34% and the presence of an equal-sized shear opening reduced the capacity by 44%, compared with the control slabs. Previous work[9–10] has also established the effects of the *a/d* and other parameters on the strength of hollow-core slabs.

Studies on reinforced concrete and prestressed concrete elements using commercial finite element method software have shown good agreement with the experimental results. Wang[11] evaluated the shear capacity of hollow-core slabs using finite element method software and found that the service load capacities of slabs observed from the numerical study matched the experimental results well. Barbosa and Riberio[12] evaluated the consequences of small changes in the modeling of reinforced concrete beams using commercial finite element method software. They used various crushing and cracking of concrete models along with the elastic and plastic properties of steel. They concluded that a good nonlinear curve of concrete in compression is important in predicting the response of the beams. Hegger et al.[13] conducted a finite element analysis of a hollow-core slab assembly on slender beams. They observed that the initial stiffness and shear deformations of the section were well captured by the finite element models (FEMs). Brunesi and Nascimbene[14] evaluated the shear capacity of hollow-core slabs using nonlinear finite element analysis. They observed that the current codes do not accurately predict shear capacity and that FEMs are better suited for accurate predictions of the shear capacity and cracking behavior of these slabs. Previous research on the bond between concrete and reinforcement[15–18] indicates that the response of the structures is not significantly affected by bond-slip behavior under small deflections. However, they found that the FEM predictions were slightly off from the test results under larger deflections when bond-slip effects were ignored. A review of the literature indicates that commercial finite element method software can be used to predict the response of various reinforced concrete and prestressed concrete elements with reasonable accuracy.

Research significance

Hollow-core slabs typically have a width of 1200 mm (47 in.) and are constructed as simply supported elements. The boundary conditions and width-to-length ratio make hollow-core slabs behave as one-way slabs. Provisions for openings or cutouts in slabs are commonly encountered at construction sites, but there are no code provisions at present that exactly quantify the effects of openings on the behavior and capacity of hollow-core slabs. The codes also do not specify any steps to mitigate the effects of openings. It is therefore crucial to evaluate the effects of openings in hollow-core slabs to better understand and use these slabs. Although previous research[6–8] has established the detrimental effects of openings on such precast concrete slabs, only a few parameters were considered for the evaluation. The main aim of this study is to evaluate the effects of openings located in flexure- and shear-dominated zones, along with various other parameters, using FEMs. The common method of designing hollow-core slabs with openings is to provide additional strands equal to the number of strands cut for the opening and distribute these additional strands in the adjacent webs. The present study evaluates the efficacy of this design practice. The parametric study includes the effects of other parameters, such as opening size and *a/d*.

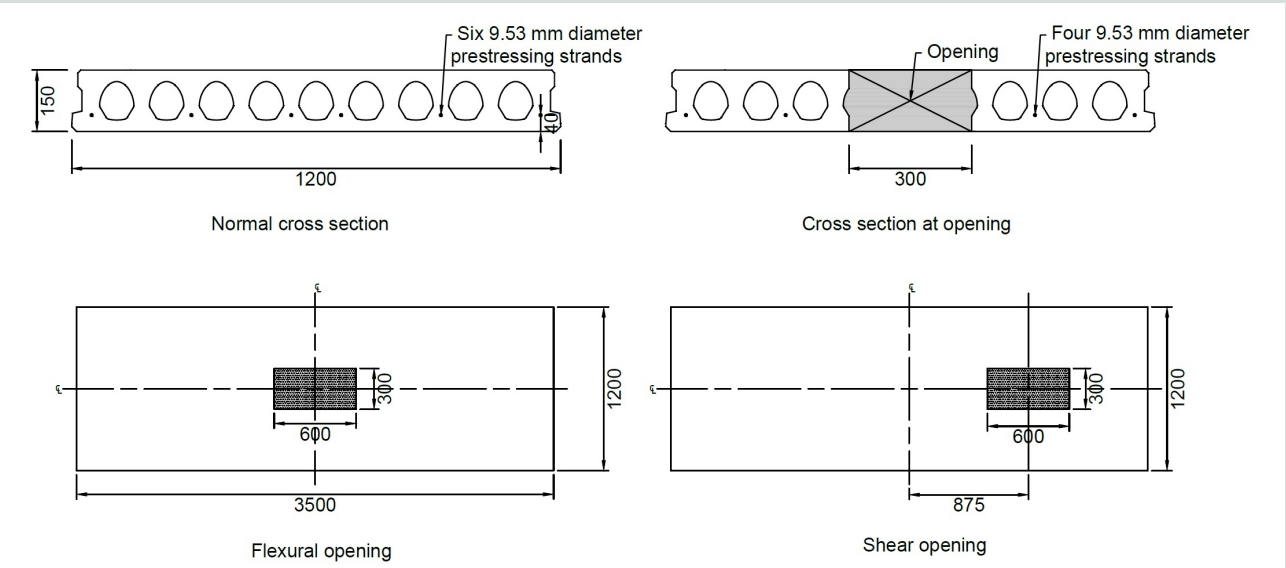

Figure 1. Cross-sectional details and plan view of slabs with openings. Note: All dimensions are in millimeters. 1 mm = 0.0394 in.

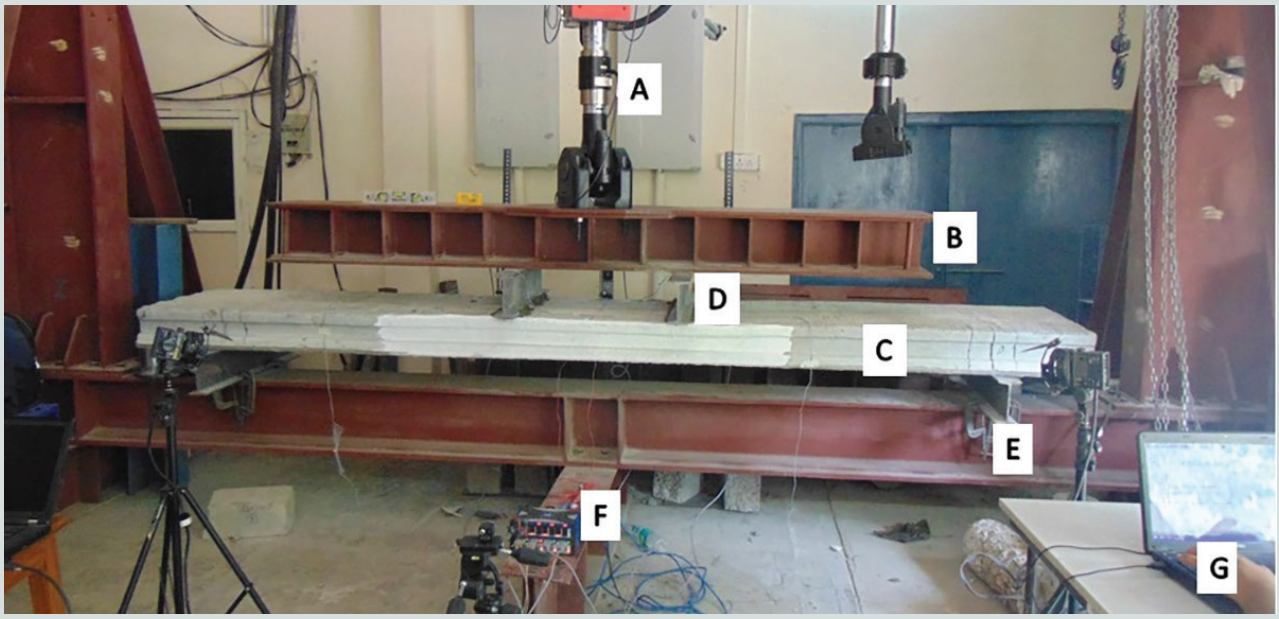

Figure 2. Test setup. Note: A = 250 kN (56 kip) actuator; B = spreader beam; C = 3.5 m (11.4 ft) hollow-core slab; D = transverse I-beams; E = support I-beams; F = data acquisition system; G = laptop.

Experimental program

Overview

A brief overview of the test procedure is given here; complete details of the test setup, loading procedure, and the behavior of specimens are provided elsewhere.[6–8] Six full-scale hollow-core slabs were tested to evaluate the effects of flexural and shear openings. All of the slabs had the same cross-sectional details (**Fig. 1**). Each slab was 150 mm (5.9 in.) deep, 1200 mm (47 in.) wide, and 3500 mm (11.5 ft) long. The slabs were prestressed with six 9.53 mm (0.375 in.) diameter prestressing strands with a prestressing jacking force of 70 kN (16 kip). One 300 × 600 mm (12 × 24 in.) opening was provided, either at the midspan location (flexural opening) or at the shear span location (shear opening) (Fig. 1). Two strands were cut at the opening location. Two *a/d* values were chosen to represent the flexure- and shear-dominated behaviors of slabs. The specimens were divided into two series based on *a/d*. In series I, the slabs were tested at a low *a/d* of 3.5; in series II they were tested at a high, flexure-dominated *a/d* of 7.5. The specimen names were derived by listing the *a/d* value followed by the opening type [3.5 or 7.5 for *a/d* and NO (no opening), FO (flexural opening), and SO (shear opening) for opening type]. The prestressing strands at the opening location were cut just before the start of the test to avoid cracking during transportation from the casting yard to the test frame. The slabs were tested in a four-point bending configuration at different *a/d* values. **Figure 2** shows the test setup.

Test procedure

Figure 2 illustrates the components used in the test setup. A 250 kN (56 kip) hydraulic actuator was used to apply the load. The actuator load was transferred to the specimens through a single longitudinal rigid steel spreader beam with web stiffeners. The load from the spreader beam was transferred to the slab through two transverse I-beams as distributed line loads along the width of the slab. High-strength cement mortar was used between the two transverse spreader I-beams and the slab to eliminate surface irregularities and to provide a smooth surface to avoid any possible stress concentrations. End supports included rigid I-beams stiffened with transverse stiffeners. Loading was applied monotonically in displacement control mode at a rate of 0.05 mm/sec (0.0019 in./sec). Loading was intermittently paused to observe and mark the crack propagation and failure progression of the tested specimen. The midspan deflection of the slabs was measured using linear variable differential transformers (LVDTs). Load-versus-midspan deflection plots were obtained for all slabs. Strain gauges were installed on the prestressing strands at the midspan location to measure the strain variation while testing.

Finite element modeling

Modeling details

The six tested specimens were modeled using commercial finite element method software to calibrate the models with experimental load-displacement curves. The exact geometry of the slabs was modeled by importing the cross sections from computer-aided design drawings. Figure 1 shows that the slabs with no openings or with flexural openings at the midspan location or with a shear opening at one end. Due to the symmetry of the slabs with no opening or flexural opening along the length, only half of the slab was modeled, thereby reducing the computational time. For the slabs with shear openings, the full slab was modeled. The models include the nonlinear constitutive stress-strain curves for concrete and

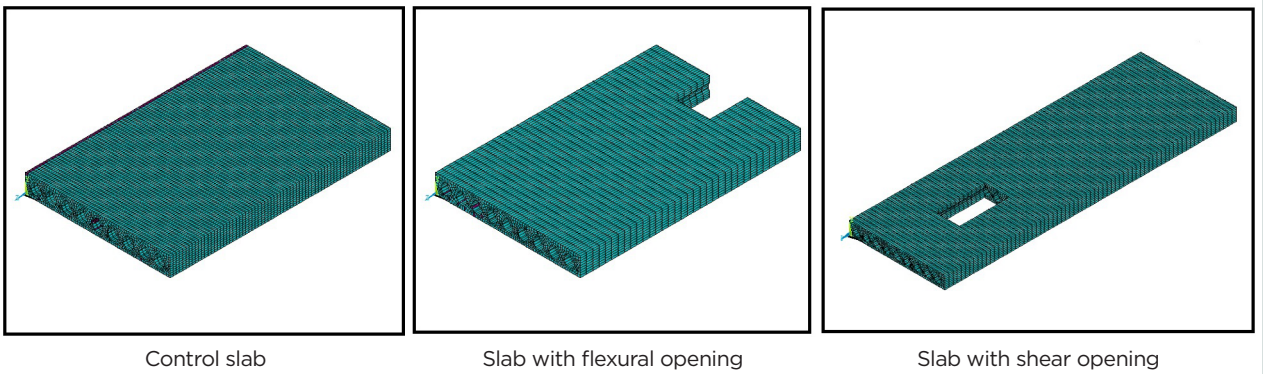

Figure 3. Finite element model of hollow-core slabs with various openings.

steel. The developed FEMs also include cracking and crushing of concrete and yielding of prestressing steel strands.

Figure 3 shows the isometric view of the modeled slabs. The concrete elements were modeled using a specialized built-in eight-node element. This element has three translational degrees of freedom at each node and is capable of cracking and crushing, which makes it a suitable element to represent the actual behavior of concrete elements. The prestressing strands were modeled using a two-dimensional truss element. This element has two translational degrees of freedom at each node. The prestressing strands were modeled to have perfect bond with concrete. Previous research on the interfacial property of concrete and reinforcement[15–18] has shown that the response of the structures will not be significantly affected by bond-slip behavior under small deflections. Mesh sensitivity analysis was performed for the slabs and the optimum finite element mesh size was achieved. An element size of 25 mm (1 in.) was used for the analysis. This is also in line with the optimum mesh size recommendations given in the literature.[19]

Material models

The following assumptions were made for the materials considered in the model: the materials are rate-independent and homogeneous, effects of temperature and moisture are negligible, and time-dependent characteristics such as creep and relaxation are not taken into account. The developed FEMs had the same material properties as those of the actual tested specimens. The cylinders were tested in the laboratory to obtain the strength of concrete on the test day. The average cylinder strength of concrete was found to be 34 MPa (4.9 ksi). The elastic modulus and Poisson's ratio of concrete were taken as 27,800 MPa (4031 ksi) and 0.2 respectively, as per ACI 318-11.[20] The nonlinear stress-strain

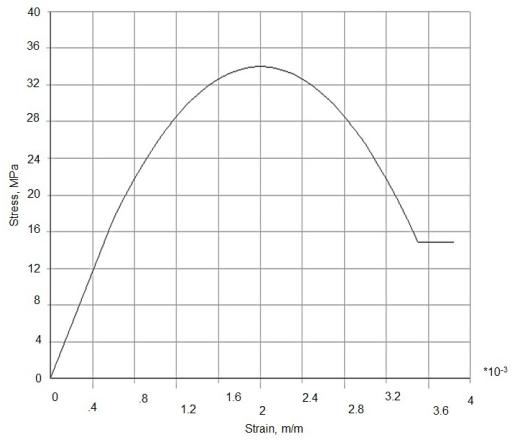

Concrete in compression

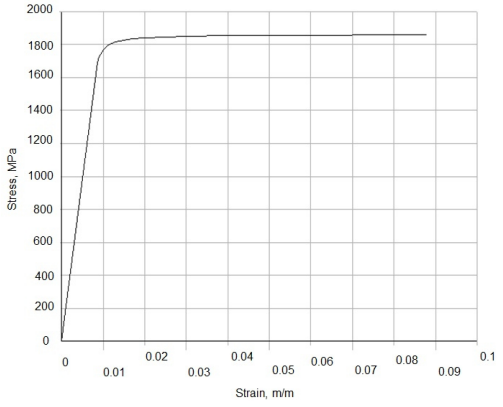

Prestressing strands

Figure 4. Material model stress-strain curves. Note: 1 m = 3.281 ft; 1 MPa = 0.145 ksi.

behavior of concrete under compression was modeled using the available analytical model[21] (**Fig. 4**). Equation (1) is the governing equation.

$$f_c = f_c'\left[\frac{2\varepsilon_c}{\varepsilon_{co}} - \left(\frac{\varepsilon_c}{\varepsilon_{co}}\right)^2\right] \text{ for } 0 \le \varepsilon_c \le \varepsilon_{co} \quad (1)$$

where

f_c = concrete compressive stress

f_c' = specified compressive strength of concrete

ε_c = concrete strain

ε_{co} = concrete strain at peak stress given by $f_c' = 2f_c'/E_c$

E_c = Young's modulus of concrete

A shear transfer coefficient β_t was introduced to the model to represent the shear strength reduction factor for subsequent load transfer after the cracks have formed. If the crack closes, then compressive stresses normal to the crack plane will be transmitted across the crack and a shear transfer coefficient β_c for a closed crack is introduced. Typical shear transfer coefficients range from 0.0 to 1.0, with 0.0 representing a smooth crack (complete loss of shear transfer) and 1.0 representing a rough crack (no loss of shear transfer). In the present analysis, values of 0.1 and 0.6 were used for open and closed shear transfer constants, respectively, after various trials. The cracking and crushing properties of concrete were given as the uniaxial tensile and compressive strengths of concrete. When the element is cracked or crushed, a small amount of stiffness is added to the element for numerical stability and defaults to 1.0×10^{-6}. The uniaxial tensile strength of concrete was taken as 7% of cylinder compressive strength.

Equation (2) expresses the criterion for failure of concrete due to a multiaxial stress state.[17]

$$\frac{F}{f_c'} - S \ge 0 \quad (2)$$

where

F = function of principal stresses in element

S = failure surface defined in terms of principal stresses

The details of function F and failure surface S can be found in the work by Willam and Warnke.[22] The stress-strain curve of prestressing strands was modeled by the equation proposed by Ramberg and Osgood,[23] with an initial elastic modulus of 197 GPa (28,400 ksi) and Poisson's ratio of 0.3 (Fig. 4). The yield stress was taken as 1690 MPa (245 ksi).

Loading and boundary conditions

Care was taken to create boundary conditions in the FEMs that were like those of the actual test conditions. The bottom nodes on the left end of the slabs were pinned with restraints in the vertical direction. Symmetric boundary conditions were applied to the area at the right end of the model, where applicable. Downward displacement was applied to the top surface nodes at a distance from supports, calculated based on the chosen *a/d*. Downward deflection was applied to the full line of nodes until the failure of the slab resembling a displacement-controlled load application. The displacement was increased in small increments after cracking to avoid convergence difficulties.

Phased analysis and failure criterion

To simulate the exact behavior of the tested slabs, a phased analysis was conducted. In phased analysis, the results of the previous phase act as input for the subsequent phases. In this study, the analysis was conducted in two phases. In the first phase, the prestress in the strands was applied and the release of prestressing force created an upward deflection (camber) in the slab, resulting in the development of tensile stress at the top and compressive stress at the bottom layers (**Fig. 5**).

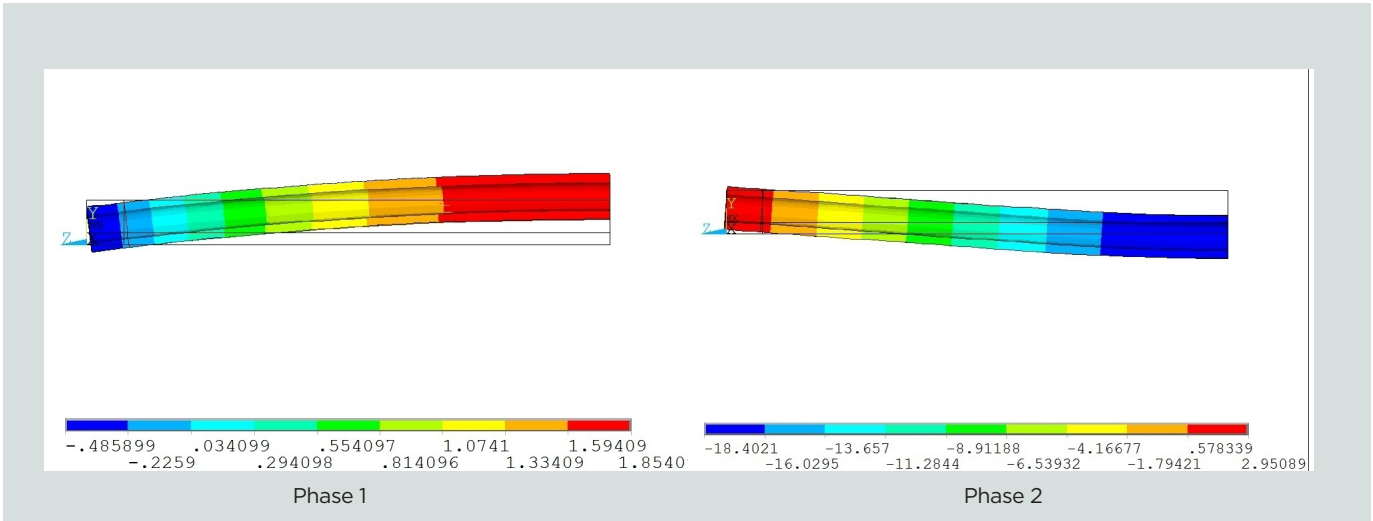

Figure 5. Deflection of slabs in phased analysis. Note: All dimensions are in millimeters. 1 mm = 0.0394 in.

In the second phase, downward displacement was applied on the top surface nodes at a distance from support nodes based on the chosen *a/d* (Fig. 5). The analysis was stopped when the convergence criterion was not met in the analysis or the strain in strands reached its rupture strain. In the present study, a displacement convergence tolerance of 5% was used. The vertical reaction was plotted against the vertical deflection of midspan nodes to generate load-deflection curves.

Analytical predictions

ACI equations

The theoretical cracking and failure capacities of the tested slabs were estimated using the equations given in ACI 318-11.[20] The flexural capacity was calculated based on assumptions given in section 10.2 of ACI 318-11. The nominal shear capacity of members without shear reinforcement depends only on concrete contribution V_c. ACI 318-11 has no specific provisions for the shear resistance of hollow-core slabs; the appropriate way to determine V_c is to follow provisions that deal with the shear strength of prestressed members. The code has two specific types or modes for concrete shear cracking (that is, web shear and flexure shear), and the smaller of the two values is considered to be the governing value for concrete shear strength V_c. Equation (3) determines the flexural-shear resistance of concrete V_{ci}.

$$V_{ci} = 0.05\lambda\sqrt{f'_c}b_w d_p + V_d + \frac{V_i M_{cre}}{M_{max}} \geq 0.17\lambda\sqrt{f'_c}b_w d_p \quad (3)$$

where

λ = modification factor that accounts for density of concrete (1 for normalweight concrete)

b_w = sum of minimum width of webs across the slab section

d_p = depth measured to the centroid of flexural reinforcement, or 0.80h, whichever is greater

h = height of section

V_d = shear force at the section due to unfactored dead loads only

V_i = factored shear force at the considered section due to externally applied loads (superimposed dead and live loads)

M_{cre} = cracking moment for the considered section due to externally applied loads

M_{max} = factored moment at the considered section due to externally applied loads

Equation (4) calculates M_{cre}.

$$M_{cre} = \left(0.5\lambda\sqrt{f'_c} + f_{pe} - f_d\right)\frac{I}{y_t} \quad (4)$$

where

f_{pe} = stress in the bottom fiber because of prestressing after all losses

f_d = stress due to unfactored dead load at bottom fiber

I = second moment of inertia of section

y_t = distance of farthest tensile fiber from centroid of section

The web-shear resistance of concrete V_{cw} is calculated from Eq. (5).

$$V_{cw} = \left(0.29\lambda\sqrt{f'_c} + 0.3f_{pc}\right)b_w d_p \quad (5)$$

where

f_{pc} = compressive stress due to prestress at the centroid of the cross section

Table 1 gives the predictions from the ACI 318-11 equations. The code equations can predict the flexural and shear capacities of the control slabs with reasonable accuracy. However, they could not accurately predict the capacity of the slabs with openings. Modifications to the code equations are required when they are used to predict the capacity of slabs with openings. Because the percentage deviation from the experimental results is higher for the ACI 318-11 equations, finite element analysis predictions are relied on for further capacity evaluations.

Results and discussion

Midspan deflection of the tested slabs measured using LVDTs was plotted against the actuator load to get the experimental load-deflection response of the slabs. Similarly, the deflection of nodes at the midspan location in all of the load steps was plotted against the vertical reaction at the supports to get the load-deflection curves in the FEM. **Figures 6** and **7** compare the FEM results with the experimental results. The experimental response of each specimen along with the FEM response is explained in the following sections.

Specimens in series I

Figure 6 compares the load and midspan deflection responses of all three slabs in series I. In the experimental results, the control slab 3.5-NO-C had a linear behavior at the beginning of loading and had an initial crack at a load of 129 kN (29.0 kip) between the loading point and the support. This cracking resulted in a load drop to 113 kN (25.4 kip). On further loading, a second load drop was observed at 161 kN (36.2 kip) due to cracking at the other end of the specimen. The slab had symmetrical cracking until a crack turned into a major diagonal shear crack on one side. The slab failed with a sudden drop in the load resistance in brittle shear failure mode. The slab had an ultimate capacity of 181 kN (40.7 kip). In the FEM, initial cracking occurred at a load of

Table 1. Results of specimens in series I

Specimen	Series I			Series II		
	3.50-NO-C	3.50-FO-C	3.50-SO-C	7.5-NO-C	7.5-FO-C	7.5-SO-C
Experimental cracking load, kN	129.6	80.5	70.5	57.3	35.3	42
Cracking load predicted by finite element analysis, kN	116.8	75.5	68.0	53.6	32.5	52.5
Cracking load predicted by ACI 318-11, kN	131.5	90.2	90.2	61.0	42.8	48.4
Experimental cracking load displacement, mm	4.3	4.3	3.8	4.4	4.1	3.6
Cracking load displacement predicted by finite element analysis, mm	4.1	4.1	3.9	3.9	3.7	4.3
Experimental peak load, kN	180.7	156.4	101.5	99.7	65.9	64.1
Peak load predicted by finite element analysis, kN	185.0	141.0	108.0	99.0	65.0	68.0
Peak load predicted by ACI 318-11, kN	160	140	114	95.1	65.5	69.1
Percentage deviation of finite element peak load from experimental peak load, %	2.3	-9.8	6.4	-1	-1	6.4
Percentage deviation of ACI 318-11 peak load from experimental peak load, %	-11.5	-9.9	12.3	-4.1	-1	7.8
Experimental peak load displacement, mm	20.7	56.5	24.2	67.5	56.3	34
Peak load displacement predicted by finite element analysis, mm	19.5	59.8	25.7	40.3	50.7	15.7
Experimental stiffness at cracking, kN/mm	30.1	18.7	18.8	13.1	8.6	11.6
Stiffness at cracking predicted by finite element analysis, kN/mm	28.5	18.4	17.4	13.7	8.8	12.2

Note: 1 mm = 0.0394 in.; 1 m = ft; 1 kN = 0.225 kip.

116.3 kN (26.15 kip). The precracking stiffness was similar to the experimental response. A sudden load drop was not observed in the FEM after cracking due to continuum modeling of concrete in the FEMs. A peak load of 185 kN (41.6 kip) was reached before the analysis was stopped due to convergence difficulties.

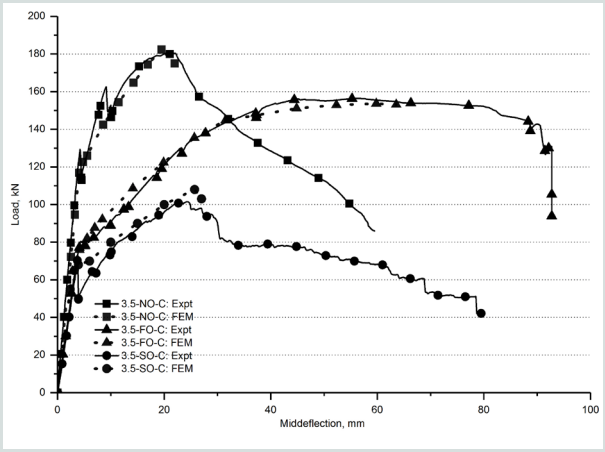

Figure 6. Comparison of experimental and FEM results: series I. Note: Expt = experimental; FEM = finite element model. 1 mm = 0.0394 in.; 1 kN = 0.225 kip.

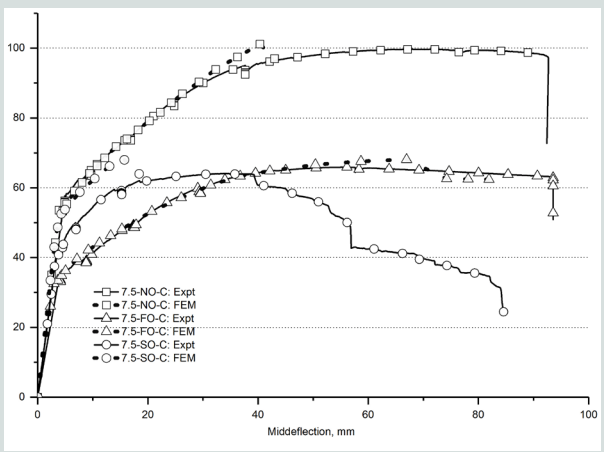

Figure 7. Comparison of experimental and FEM results: series II. Note: Expt = experimental; FEM = finite element model. 1 mm = 0.0394 in.; 1 kN = 0.225 kip.

Figure 8. Failure modes of specimens.

The second specimen with a flexural opening and tested at an *a/d* of 3.5 (specimen 3.5-FO-C) had initial flexural cracking in the constant moment zone at 80.5 kN (18.1 kip). The first crack occurred at the midspan location at the corner of the opening, though the chosen *a/d* was a shear-dominated one, crack distribution occurred in the opening location only. On further loading, the resistance steadily increased due to the contribution of strands. The slab resisted a peak load of 156 kN (35.1 kip) with a corresponding displacement of 56.5 mm (2.22 in.) and finally failed due to crushing of the top concrete at the corner of the opening. Due to the presence of the opening, there was a 14% reduction in peak capacity compared with the control slab. However, there was an increase in displacement corresponding to the peak load due to the change in failure mode. The provision of a flexural opening changed the failure mode from brittle shear to ductile flexure. This is due to the weak link in the constant moment zone, which had a lower moment capacity than the shear capacity of the full cross section in the constant shear zone. The FEM of this specimen predicted a cracking load of 75.5 kN (17.0 kip) and peak load of 141 kN (31.7 kip). The FEM also had initial cracking at the corner of the opening, similar to the experimental results. The precracking and postcracking responses were accurately predicted by the FEM (Fig. 6). The FEMs also accurately predicted the increase in peak load deflection and ultimate deflection of specimen 3.5-FO-C.

The last specimen in series I was the slab with a shear opening and tested at an *a/d* of 3.5 (specimen 3.5-SO-C). Due to an opening in the shear zone, the first crack occurred in the opening location in the constant shear zone at a load of 70.5 kN (15.8 kip) and caused a sudden drop in load to 50 kN (11 kip). On further loading, the load picked up to a peak value of 101.5 kN (22.82 kip) before the slab failed in brittle shear mode. Provision of a shear opening led to 44% reduction in capacity of the slab. The FEM of specimen 3.5-SO-C predicted a cracking load of 68 kN (15 kip) and a peak load of 108 kN (24.3 kip). The FEM predicted a slightly stiffer postcracking response of the slab with shear opening. The experimental specimen had a sudden load drop after the initial cracking and load resistance picked up from the decreased load. **Table 1** summarizes the results of this series.

Specimens in series II

The second series of slabs were tested at a flexural *a/d* of 7.5. Specimen 7.5-NO-C, with no opening, served as the control slab for this series. The slab had an initial crack in the constant moment zone at a load of 57 kN (13 kip). Distributed cracks occurred in the constant moment zone before the peak load was attained. A peak load of 99 kN (22 kip) was reached after considerable yielding of strands at a displacement of 67 mm (2.6 in). This slab finally failed due to crushing of compression concrete just below the loading point. The FEM also had initial cracks at the midspan location at a load of 53.6 kN (12.1 kip), and cracks propagated toward the compression zone on further loading. The FEM also predicted a peak load of 99 kN with a close prediction of precracking and postcracking stiffness.

Specimen 7.5-FO-C, tested at an *a/d* of 7.5 and with a flexural opening, had the first crack at the corner of the opening at a load of 36 kN (8.1 kip). On further loading, unlike the control slab, crack distribution took place only in the opening zone. A peak load of 65.9 kN (14.8 kip) was reached before the slab failed due to crushing of the top concrete at the corner of the opening. Provision of a flexural opening led to a 34% reduction in capacity of the slab. Even in the FEM of specimen 7.5-FO-C, initial cracking occurred at the corner of the opening at a load of 32.5 kN (7.31 kip). The FEM predicted a peak load of 65 kN (15 kip) with cracks concentrated at the opening location.

The last specimen of the experiments was the slab with a shear opening tested at an *a/d* of 7.5 (specimen 7.5-SO-C). Although the chosen *a/d* was flexure-dominated, initial cracking occurred in the constant shear zone due to the presence of the opening. On further loading, the initial crack developed into a major shear crack, leading to diagonal shear failure of the slab. The slab resisted a peak load of 64.1 kN (14.4 kip).

The FEM of this slab also had initial cracking in the opening location. A peak load of 68 kN (15 kip) was predicted by the FEM. The predicted peak load values in all of the cases were within 7% accuracy. Figure 7 compares the load and deflection curves of the slabs in series II, and **Table 1** lists the corresponding values.

Failure modes

Figure 8 shows the failure modes of slabs tested in series I and II. In series I, the slabs were tested at a low shear-dominated *a/d*. The control slab with no opening (specimen 3.5-NO-C) and the slab with a shear opening (specimen 3.5-SO-C) both failed in shear mode. The slab with a flexural opening (specimen 3.5-FO-C) failed due to crushing of concrete at the corner of the opening in ductile flexural mode. In series II, specimen 7.5-NO-C failed due to crushing of concrete below the loading point. Specimen 7.5-FO-C failed due to crushing of concrete at the opening location, and specimen 7.5-SO-C failed in diagonal shear mode.

The FEMs predicted cracking patterns similar to the experiment results. **Figure 9** compares the failure propagation of a few specimens. Figure 9 shows the initial cracking of the control specimen with no opening in series I. The experimental specimen had initial cracking in the constant shear zone, and the FEM predicted cracking at the same location. The series II control slab with no opening (specimen 7.5-NO-C) had initial cracking in the constant moment zone, and multiple cracks formed before failure occurred due to crushing of concrete below the load point (Fig. 9). The FEM predicted a response similar to that of the experimental results. In the specimen with an opening, cracking started from the corner of the opening due to stress concentration. In the FEM, initial cracking also occurred at the corner of the opening (Fig. 9). The developed FEMs accurately predicted the load-deflection response, cracking and peak-load values, and failure patterns. These models can further be used for parametric studies to evaluate the effects of different variables, such as the size of the opening, *a/d*, and the number of prestressing strands in adjacent webs, because testing full-scale specimens for all variables is not practical or economically feasible.

Parametric studies

Parameters for the study

A parametric study was performed using the calibrated FEMs to evaluate the effects of various parameters on the behavior of hollow-core slabs with openings. Among the various parameters considered, the most important one was to evaluate the current design procedure of hollow-core slabs with openings. Designers typically compensate for the effects of openings in hollow-core slabs by providing a number of additional strands in the adjacent webs equal to the number of strands cut. This case was considered in the parametric study to evaluate the ability of additional strands in webs to restore the hollow-core slab's capacity that is lost due to openings. Along with this parameter, the effects of the *a/d* and of the opening size were also considered in the study. The cross section and materials used to calibrate experimental results were used for the parametric study.

Effects of opening size

Two different opening sizes of 300 × 600 mm (12 × 24 in.) and 500 × 600 mm (20 × 24 in.) were chosen to study the effects of opening size on the behavior of hollow-core slabs. The location of the opening was varied between the flexure-dominated midspan zone and the shear-dominated end zone. The control slab had six 9.53 mm (0.375 in.) diameter prestressing strands that were prestressed up to 70 kN (16 kip) force. **Table 2** summarizes the specimens for this variable.

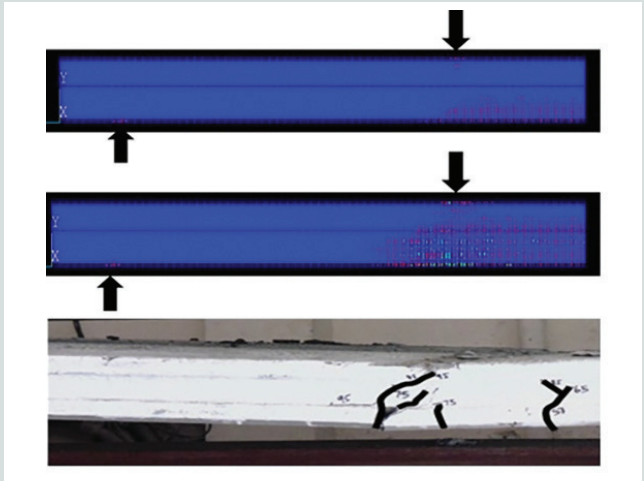

Comparison of failure progression in flexure-dominated specimens

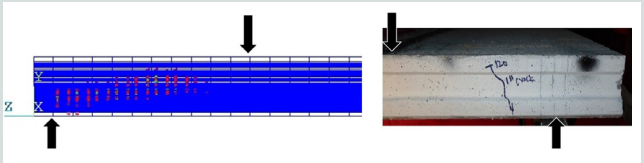

Comparison of shear cracks in specimens

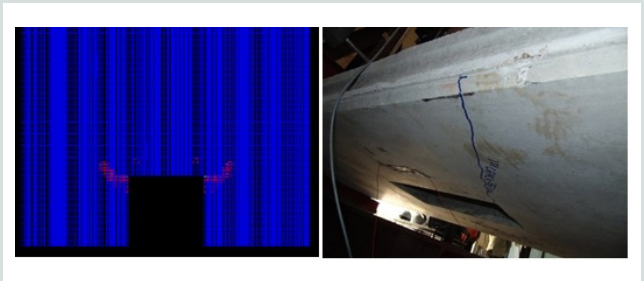

Comparison of initial cracks at corner of opening

Figure 9. Comparison of failure modes

Table 2. Specimens for effects of opening size

Specimen name	Opening size, mm	Opening location	*a/d*	Number of strands at normal location	Number of strands at opening location	Predicted peak load, kN
2-NO-6S: FEM	n/a	None	2.0	6	n/a	328
2-FO1-6S: FEM	300 × 600	Flexure zone	2.0	6	4	224
2-SO1-6S: FEM	300 × 600	Shear zone	2.0	6	4	260
2-FO2-6S: FEM	500 × 600	Flexure zone	2.0	6	4	207
2-SO2-6S: FEM	500 × 600	Shear zone	2.0	6	4	203
3.5-NO-6S: FEM	n/a	None	3.5	6	n/a	184
3.5-FO1-6S: FEM	300 × 600	Flexure zone	3.5	6	4	124
3.5-SO1-6S: FEM	300 × 600	Shear zone	3.5	6	4	144
3.5-FO2-6S: FEM	500 × 600	Flexure zone	3.5	6	4	112
3.5-SO2-6S: FEM	500 × 600	Shear zone	3.5	6	4	128
8.5-NO-6S: FEM	n/a	None	8.5	6	n/a	93
8.5-FO1-6S: FEM	300 × 600	Flexure zone	8.5	6	4	60
8.5-SO1-6S: FEM	300 × 600	Shear zone	8.5	6	4	75
8.5-FO2-6S: FEM	500 × 600	Flexure zone	8.5	6	4	53
8.5-SO2-6S: FEM	500 × 600	Shear zone	8.5	6	4	69

Note: *a* = shear span; *d* = depth of section; FEM = finite element model; n/a = not applicable. 1 mm = 0.0394 in.; 1 kN = 0.225 kip.

In total, 15 specimens were analyzed. Increasing the opening width from 300 to 500 mm reduced the cross-sectional area of concrete by an additional 18% and did not lead to additional curtailment of strands. Three *a/d* values of 2, 3.5, and 8.5 were chosen to evaluate the effects of opening size under different shear-to-moment ratios.

Figure 10 shows the results from this study. At a low *a/d* of 2, increasing the opening size in the flexural zone did not alter the cracking load and postcracking stiffness but decreased the peak load by 7.5% (Fig. 10). However, in the case of the slab with the shear opening at a low *a/d* of 2, increasing the opening size decreased both the precracking and postcracking stiffness of the slab. It also led to a decrease in peak load by 22%. This indicates that increasing the opening size in a shear-dominated zone in low *a/d* slabs is more detrimental than increasing the opening at the midspan location.

Table 3. Specimens for effects of *a/d*

Specimen name	Opening size, mm	Opening location	*a/d*	Number of prestressing strands at normal location	Sectional capacity predicted by FEM, kN-m
2-NO-10S: FEM	n/a	None	2	10	57.3
2-FO1-10S: FEM	300 × 600	Flexure zone	2	10	86.6
2-SO1-10S: FEM	300 × 600	Shear zone	2	10	51.9
3.5-NO-10S: FEM	n/a	None	3.5	10	60.5
3.5-FO1-10S: FEM	300 × 600	Flexure zone	3.5	10	46
3.5-SO1-10S: FEM	300 × 600	Shear zone	3.5	10	51.5
8.5-NO-10S: FEM	n/a	None	8.5	10	82.6
8.5-FO1-10S: FEM	300 × 600	Flexure zone	8.5	10	54.2
8.5-SO1-10S: FEM	300 × 600	Shear zone	8.5	10	65

Note: a = shear span; d = depth of section; FEM = finite element model; n/a = not applicable. 1 mm = 0.0394 in.; 1 m = 3.281 ft; 1 kN = 0.225 kip.

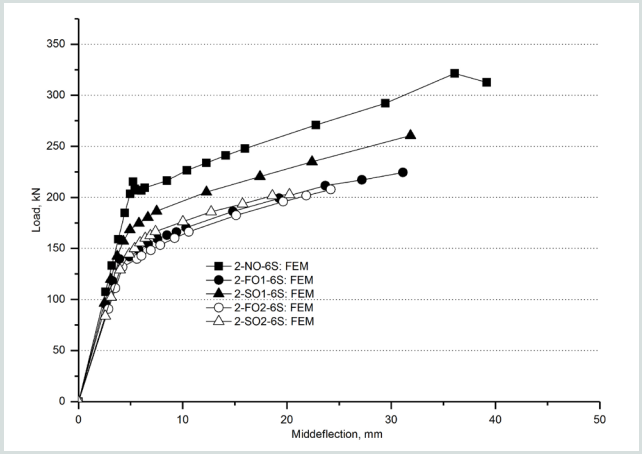

a/d = 2

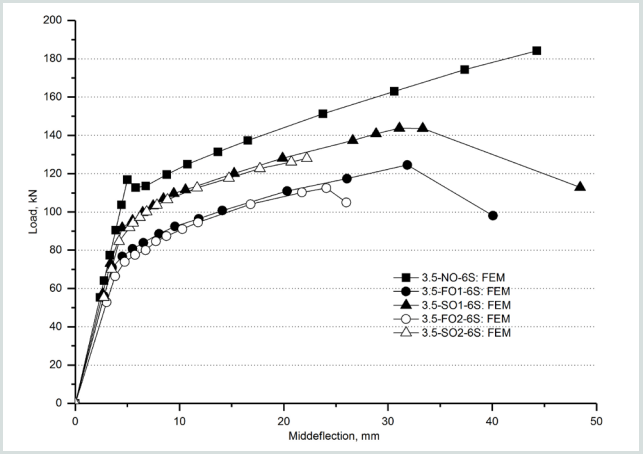

a/d = 3.5

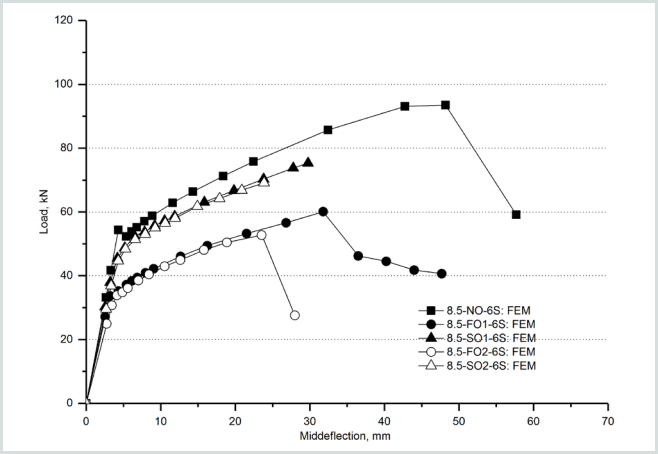

a/d = 8.5

Figure 10. Effects of opening size. Note: *a* = shear span; *d* = depth of section; FEM = finite element model. 1 mm = 0.0394 in.; 1 kN = 0.225 kip.

The effects of varying *a/d* values from 3.5 to 8.5 indicated that increasing the opening size did not alter the cracking load and postcracking stiffness but decreased the peak load by less than 10%. Table 2 gives the peak load values. It can be concluded from Fig. 10 that if the openings in the slabs result in the reduction of the concrete area only, without any curtailment of strands, then the decrease in peak load capacity is minimal. Moreover, the increase in opening size also does not affect the precracking or postcracking stiffness of slabs. Care should be taken when providing openings in the shear zone of slabs at a low *a/d*, as the reduction in peak load will not be proportional to the reduction in concrete area.

Effects of the *a/d*

Nine models were developed to understand the effects of *a/d* on the behavior of slabs with and without openings. The main variable was *a/d*, which was varied from 2 to 8.5. Ten prestressing strands of 9.53 mm (0.375 in.) diameter were provided in the slab. Each strand was stressed to a force of 70 kN (16 kip). A 300 × 600 mm (12 × 24 in.) opening was provided in either the flexural zone or the shear zone to evaluate the effects of the *a/d* in hollow-core slabs with openings. Two strands were cut at the middle of the cross section for the opening. **Table 3** summarizes the specimens of this study. **Figure 11** compares the midspan bending moment with the midspan deflection of slabs with the same parameter, that is, no opening or flexural opening or shear opening. The precracking stiffness response of the slabs remained unchanged between *a/d* values of 2 and 3.5. However, it increased to a considerable value when the *a/d* was increased to 8.5. Moreover, in all cases, the peak bending moment increased as the *a/d* changed to 8.5. It can be concluded that the sectional moment capacity of hollow-core slabs decreases as the loading becomes more shear-dominated, and due care should be taken to take this effect into account.

Effects of additional strands

Two control slabs without openings and with the same dimensions and material properties but with different numbers of prestressing strands were analyzed to study the effects

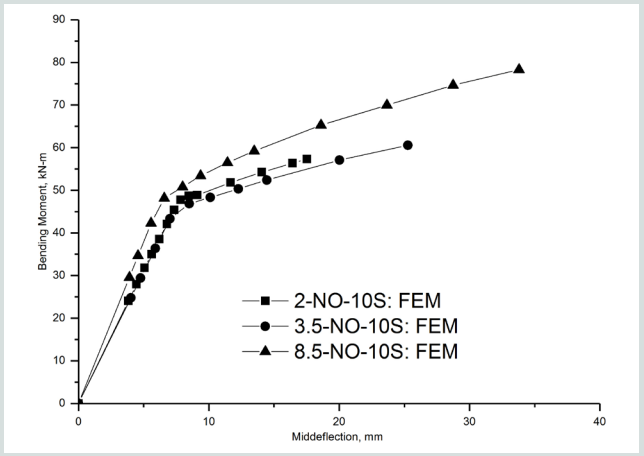

Control specimens

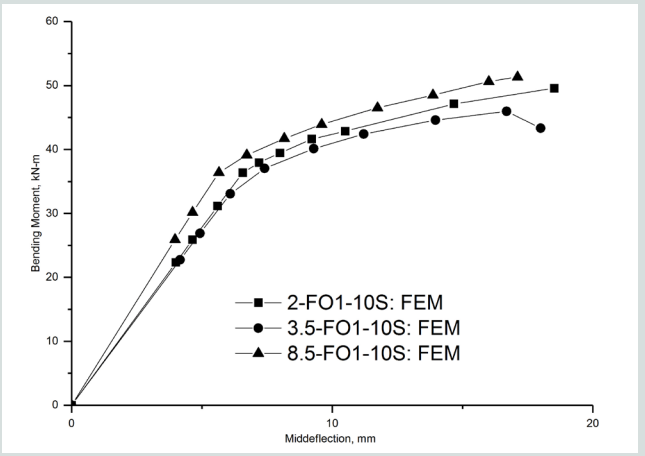

Specimens with flexural opening

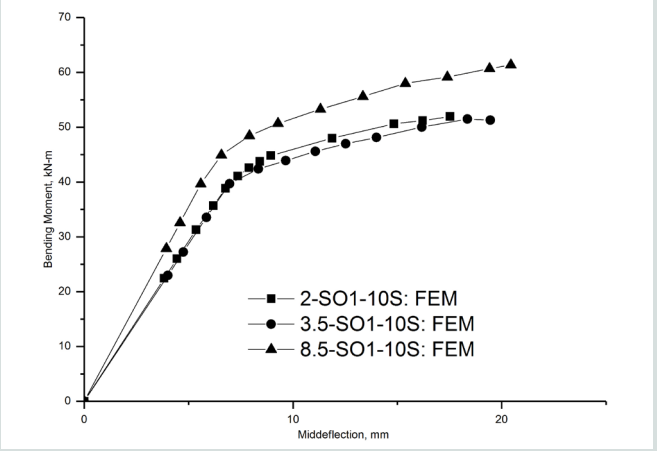

Specimens with shear opening

Figure 11. Effects of *a/d*. Note: *a* = shear span; *d* = depth of section; FEM = finite element model. 1 mm = 0.0394 in.; 1 m = 3.281 ft; 1 kN = 0.225 kip.

Table 4. Specimens for the effects of additional strands

Specimen name	*a/d*	Opening type	Number of strands at normal location	Number of strands at opening location	Peak load predicted by FEM, kN
2-NO-6S: FEM	2	No opening	6	n/a	328
2-FO2-6S: FEM	2	Flexural opening	6	4	207
2-SO2-6S: FEM	2	Shear opening	6	4	203
2-NO-10S: FEM	2	No opening	10	n/a	382
2-FO2-10S: FEM	2	Flexural opening	10	6	248
2-SO2-10S: FEM	2	Shear opening	10	6	283
8.5-NO-6S: FEM	8.5	No opening	6	n/a	93
8.5-FO2-6S: FEM	8.5	Flexural opening	6	4	53
8.5-SO2-6S: FEM	8.5	Shear opening	6	4	69
8.5-NO-10S: FEM	8.5	No opening	10	n/a	131
8.5-FO2-10S: FEM	8.5	Flexural opening	10	6	61
8.5-SO2-10S: FEM	8.5	Shear opening	10	6	90

Note: *a* = shear span; *d* = depth of section; FEM = finite element model; n/a = not applicable. 1 kN = 0.225 kip.

of providing additional strands. One control slab had six prestressing strands, and another had 10 prestressing strands. In both the cases, the strands were stressed to a jacking force of 70 kN (16 kip). Thereafter, the slabs with openings were analyzed. An opening of 500 × 600 mm (20 × 24 in.) was provided in the slab with six strands. The opening was provided such that two strands were cut in the slabs with six strands. Because two strands were cut due to the opening, two strands were added to the adjacent webs in the next set of specimens. It was planned such that the next set of specimens had six strands at the opening location. For this purpose, an opening of 500 × 600 mm was provided in the slabs with 10 strands so that after cutting four strands due to the opening, six were left out at the opening section. The results from the slabs with openings were compared with the results from the control slabs. Two *a/d* values of 2 and 8.5 were considered to evaluate this parameter under different shear-to-moment ratios. **Table 4** presents the specimens analyzed for this parameter along with the results.

Increasing the number of strands did not alter the initial stiffness of specimens with and without openings. However, it increased the cracking and peak loads along with the increase in postcracking stiffness (**Fig. 12**). From the results of the finite element analysis, it was found that increasing the number of strands in slabs with openings did not restore the stiffness lost due to the opening. Figure 12 shows six cases of analysis. Out of these curves, two of them—specimens 2-NO-6S: FEM and 8.5-NO-6S: FEM—act as reference curves for the specimens with openings and with 10 strands. Four strands were cut due to openings in the specimens with 10 strands, making the prestressing force equivalent to that of the control slabs with six strands. Figure 12 shows that increasing the prestressing strands at the opening location did not restore the lost capacity of slabs with flexural openings. The only advantage of increasing the prestressing strands is an increase in postcracking stiffness. In the case of slabs with shear openings (Fig. 12), it was observed that the capacity of a 10-strand slab with an opening at a low *a/d* of 2 is above the control slab capacity with six strands. However, in the case of a higher *a/d* of 8.5, the peak load was not restored by an increase in the number of strands. Therefore, it can be concluded that providing additional reinforcement does not restore the capacity of slabs in all cases.

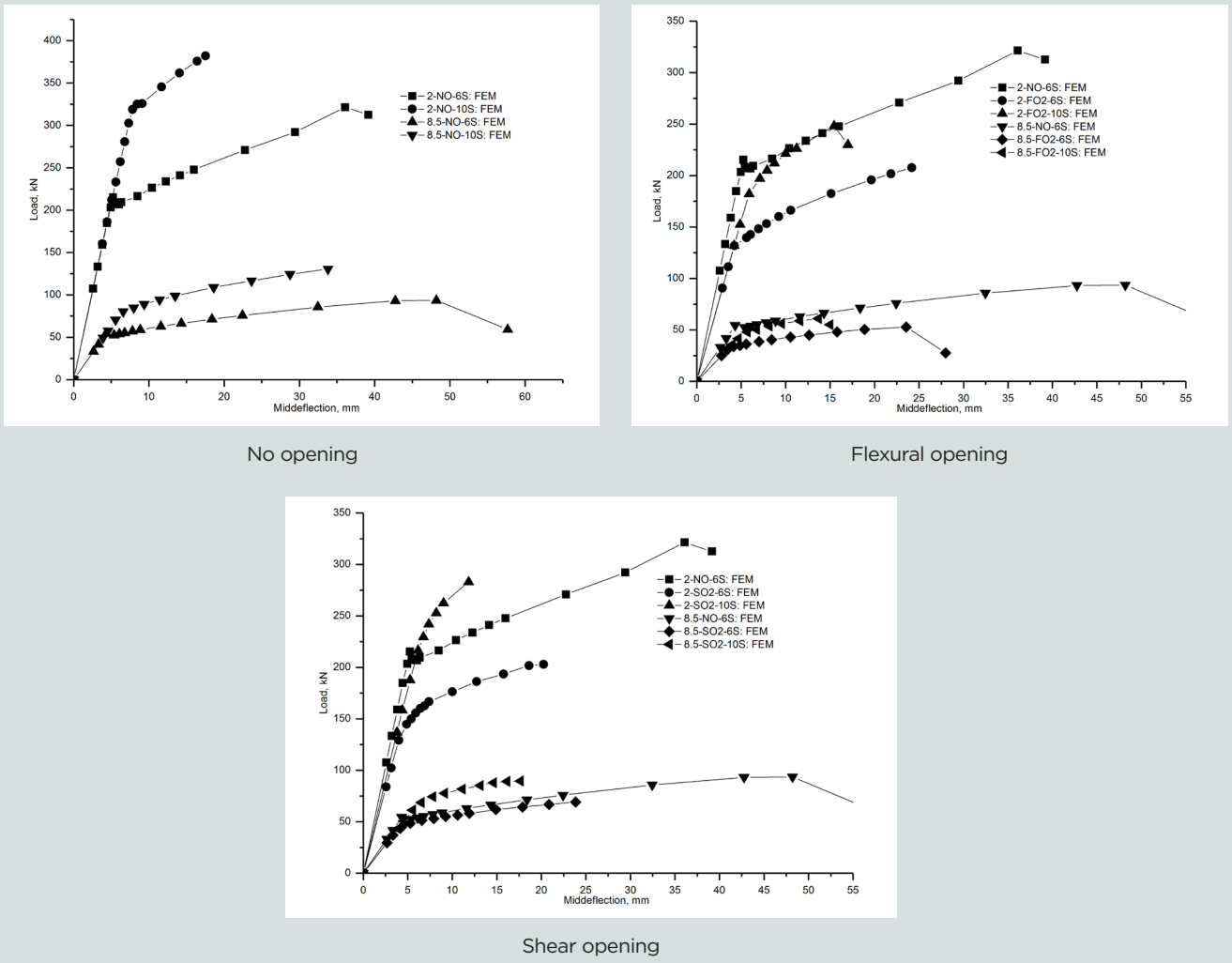

Figure 12. Effects of additional strands. Note: FEM = finite element model. 1 kN = 0.225 kip; 1 mm = 0.0394 in.

Conclusion

Three-dimensional FEMs were developed and calibrated with test data to predict the behavior of prestressed hollow-core slabs with openings. After the calibration of the developed FEMs, a parametric study was conducted to investigate the effects of opening size, *a/d*, and additional strands. The finite element analysis was conducted for limited parameters in this study. Future research could focus on the effects of other parameters, such as varying opening shapes, concrete grade, and the cross-sectional shape of the hollow-core slabs. Studying the effects of grouted keyways, load distribution, and strand development would be interesting and is scope for further work. These parametric results could be used to develop design guidelines for predicting the capacity of slabs with openings.

The following major conclusions can be drawn from the results presented in this study:

- The developed FEMs predicted the behavior of prestressed hollow-core slabs with reasonable accuracy. The ultimate strength was predicted within 7% deviation from the test results.
- Results of the finite element analysis indicate that the provision of openings reduced the strength and stiffness of the slabs, depending on the *a/d*. The reduction in strength and stiffness due to flexural opening was higher in higher *a/d* specimens, whereas the shear opening was found to be critical in specimens tested at a low *a/d*.
- Parametric results indicated that the opening size should be carefully selected based on the location of the opening. Increasing the opening size in a shear-dominated zone results in more adverse behavior than increasing the opening size at the midspan location.
- Considerations should be given while calculating the sectional capacity of slabs based on the loading conditions. It was observed that shear-dominated loading can significantly decrease the sectional capacity of hollow-core slabs both with and without openings.
- The common methodology of designing hollow-core slabs with openings, where the number of strands is increased by the number of strands cut, was found to be inconsistent in restoring the capacity of slabs with openings. A thorough case-by-case analysis of the slabs is required to evaluate the effects of openings.

References

1. Walraven, J. C., and W. P. M. Mercx. 1983. "The Bearing Capacity for Prestressed Hollow Core Slabs." *Heron* 28 (3): 1–46.
2. Becker, R. J., and D. R. Buettner. 1985. "Shear Tests of Extruded Hollow-Core Slabs." *PCI Journal* 30 (2): 40–54.
3. Pajari, M. 1998. "Shear Resistance of PHC Slabs Supported on Beams. II: Analysis." *Journal of Structural Engineering* 124 (9): 1062–73. doi:10.1061/(ASCE)0733-9445(1998)124:9(1062).
4. Hawkins, N. M., and S. K. Ghosh. 2006. "Shear Strength of Hollow-Core Slabs." *PCI Journal* 51 (1): 110–4.
5. Palmer, K. D., and A. E. Schultz. 2011. "Experimental Investigation of the Web-Shear Strength of Deep Hollow-Core Units." *PCI Journal* 56 (4): 83–104.
6. Pachalla, S. K. S., and S. S. Prakash. 2017. "Load Resistance and Failure Modes of GFRP Composite Strengthened Hollow Core Slabs with Openings." *Materials and Structures* 50 (1). doi: 10.1617/s11527-016-0883-8.
7. Pachalla, S. K. S., and S. S. Prakash. 2017. "Experimental Evaluation on Effect of Openings on Behavior of Prestressed Precast Hollow-Core Slabs." *ACI Structural Journal* 114 (2): 427–436. doi:10.14359/51689155.
8. Pachalla, S. K. S., and S. S. Prakash. 2017. "Efficient Near Surface Mounting CFRP Strengthening of Pretensioned Hollowcore Slabs with Opening – An Experimental Study." *Composite Structures* 162 (15): 28–38. doi:10.1016/j.compstruct.2016.11.072.
9. Kankeri, P., and S. S. Prakash. 2016. "Experimental Evaluation of Bonded Overlay and NSM GFRP Bar Strengthening on Flexural Behavior of Precast Prestressed Hollow Core Slabs." *Engineering Structures* 120: 49–57. doi:10.1016/j.engstruct.2016.04.033.
10. Kankeri, P., and S. S. Prakash. 2017. "Efficient Hybrid Strengthening for Precast Hollow Core Slabs at Low and High Shear Span to Depth Ratios." *Composite Structures* 170: 202–214. doi:10.1016/j.compstruct.2017.03.034.
11. Wang, X. 2007. "Study on the Shear Behavior of Prestressed Hollow Core Slabs by Nonlinear Finite Element Modelling." Master's degree thesis. University of Windsor, ON, Canada.
12. Barbosa, A. F., and G. O. Ribeiro. 1998. "Analysis of Reinforced Concrete Structures using Ansys Nonlinear Concrete Model." In *Computational Mechanics. New Trends and Applications*, S. Idelsohn, E. Oñate, and E. Dvorkin (eds.), pp. 1–7. Barcelona, Spain: Centro Internacional de Métodos Numéricos en Ingeniería.
13. Hegger, J., T. Roggendorf, and F. Teworte. 2010. "FE Analyses of Shear-Loaded Hollow-Core Slabs On Different Supports." *Magazine of Concrete Research* 62 (8): 531–541.
14. Brunesi, E., and R. Nascimbene. 2015. "Numerical Web-Shear Strength Assessment of Precast Prestressed Hollow Core Slab Units." *Engineering Structures* 102: 13–30.

15. Gan, Y. 2000. "Bond Stress and Slip Modeling in Nonlinear Finite Element Analysis of Reinforced Concrete Structures." Master's degree thesis. University of Toronto, Canada.

16. Mondal, T. G., and S. S. Prakash. 2016. "Nonlinear Finite-Element Analysis of RC Bridge Columns under Torsion with and without Axial Compression." *Journal of Bridge Engineering* 21 (2). doi:10.1061/(ASCE)BE.1943-5592.0000798.

17. Ganganagoudar, A., T. G. Mondal, and S. S. Prakash. 2016 "Analytical and Finite Element Studies on Behavior of FRP Strengthened RC Beams under Torsion." *Composite Structures* 153: 876–885. doi:10.1016/j.compstruct.2016.07.014.

18. Ganganagoudar, A., T. G. Mondal, and S. S. Prakash. 2016. "Improved Softened Membrane Model for Reinforced Concrete Circular Bridge Columns under Torsional Loading." *Journal of Bridge Engineering* 21 (7): 1–13. doi: 10.1061/(ASCE)BE.1943-5592.0000907.

19. Kim, Y. J., J. M. Longworth, R. G. Wight, and M. F. Green. 2010. "Punching Shear of Two-way Slabs Retrofitted with Prestressed or Non-prestressed CFRP Sheets." *Journal of Reinforced Plastics and Composites* 29 (8): 1206–23. doi:10.1177/0731684409103143.

20. ACI (American Concrete Institute) Committee 318. 2011. *Building Code Requirements for Structural Concrete (ACI 318-11) and Commentary (ACI 318R-11*). Farmington Hills, MI: ACI.

21. Hognestad, E. 1951. "Study of Combined Bending and Axial Load in Reinforced Concrete Members." Bulletin 399. Engineering Experiment Station, University of Illinois at Urbana-Champaign.

22. Willam, K., and E. Warnke. 1975. "Constitutive Model for the Triaxial Behavior of Concrete International Association for Bridge and Structure Engineering." In *Proceedings, International Association for Bridge and Structure Engineering*. Bergamo, Italy: International Association for Bridge and Structural Engineering.

23. Ramberg, W., and W. R. Osgood. 1943. "Description of Stress-Strain Curves by Three Parameters." Technical Note 902. National Advisory Committee for Aeronautics.

Notation

a = shear span

b_w = sum of minimum width of webs across the slab section

d = depth of section

d_p = depth measured to the centroid of prestressed reinforcement

E_c = Young's modulus of concrete

f_c = compressive stress

f'_c = specified compressive strength of concrete cylinder

f_d = stress due to unfactored dead load at bottom fiber

f_{pc} = compressive stress due to prestress at the centroid of cross section

f_{pe} = stress in the bottom fiber because of prestressing after all losses

F = function of principal stresses in concrete element

h = height of section

I = second moment of inertia of section

M_{cre} = cracking moment for the considered section due to externally applied loads

M_{max} = factored moment at the considered section due to externally applied loads

S = failure surface defined in terms of principal stresses

V_c = nominal shear capacity

V_{ci} = flexural-shear resistance of concrete

V_{cw} = web-shear resistance of concrete

V_d = shear force at the section due to unfactored dead loads

V_i = factored shear force at the considered section due to externally applied loads (superimposed dead and live loads)

y_t = distance of farthest tensile fiber from centroid of section

β_t = shear transfer coefficient after the cracks have formed

β_c = shear transfer coefficient for a closed crack

ε_c = concrete strain

ε_{co} = concrete strain corresponding to $f'_c = 2f'_c/E_c$

λ = modification factor that accounts for density of concrete

About the authors

Sameer K. S. Pachalla, PhD, is a member of the faculty at the Mahindra Ecole Centrale College of Engineering in Hyderabad, India.

S. Suriya Prakash, PhD, is an associate professor in the department of Civil Engineering at the Indian Institute of Technology Hyderabad in Telangana, India.

Abstract

Hollow-core slabs are generally used as floor elements in buildings. Provision of openings and cutouts is common in slabs due to various structural or service requirements. In many situations, these openings are provided after the slab has been erected, based on the site requirements. Design engineers typically confirm the safety of prestressed hollow-core slabs with openings based on experience or by simple stress calculations, as no design guidelines exist at present for the design of these precast concrete slabs with openings. If the openings are planned in the design phase, their effects are generally lessened by providing additional prestressing strands in the adjacent webs. This paper evaluates the effects of openings on the behavior of hollow-core slabs by experimental and finite element method studies. Three-dimensional finite element models were developed and calibrated with the experimental data. Thereafter, the effects of the provision of additional strands in adjacent webs, the shear span–to–depth ratio, and opening size were studied. The provision of additional strands in webs adjacent to an opening could not completely restore the lost capacity of hollow-core slabs due to openings. The location and size of the openings plays an important role in the strength and failure mode of the hollow-core slabs.

Keywords

Cutouts, finite element method, finite element model, hollow-core slabs, openings, shear span–to–depth ratio.

Review policy

This paper was reviewed in accordance with the Precast/Prestressed Concrete Institute's peer-review process.

Reader comments

Please address any reader comments to *PCI Journal* editor-in-chief Emily Lorenz at elorenz@pci.org or Precast/Prestressed Concrete Institute, c/o *PCI Journal*, 200 W. Adams St., Suite 2100, Chicago, IL 60606.